NLRP3 knockout in mice provided protection against Serratia marcescens-induced acute pneumonia by decreasing PD-L1 and PD-1 expression in macrophages

Kan-Yao Chen, Shu-Yan Liu, Juan-Juan Tang, Meng-Ke Liu, Xu-Yang Chen, Zhi-Peng Liu, Dominique Ferrandon, Ke-Fang Lai, Zi Li

NLRP3 knockout in mice provided protection against *Serratia marcescens*-induced acute pneumonia by decreasing PD-L1 and PD-1 expression in macrophages

Kan-yao Chen [1,5#], Shu-yan Liu [1,6#], Juan-juan Tang [1#], Meng-ke Liu [1], Xu-yang Chen [1], Zhi-peng Liu [1], Dominique Ferrandon [1,2,4], Ke-fang Lai [2*], Zi Li [1,2,3*]

[1] Sino-French Hoffmann Institute, School of Basic Medical Sciences, Guangzhou Medical University, Guangzhou, China.

[2] State Key Laboratory of Respiratory Disease, Guangzhou Institute of Respiratory Health, Guangzhou Medical University, Guangzhou, China.

[3] The Second Affiliated Hospital of Guangzhou Medical University, Guangdong Provincial Key Laboratory of Allergy & Clinical Immunology, Guangzhou Medical University, Guangzhou, China.

[4] Université de Strasbourg, RIDI UPR9022 du CNRS, F-67000 Strasbourg France.

[5] Department of Clinical Laboratory, Guangdong Provincial People's Hospital Zhuhai Hospital, Zhuhai, China.

[6] Department of Clinical Laboratory, Guangzhou Twelfth People's Hospital, Guangzhou, China.

Correspondence: klai@163.com; lizi1002@gzhmu.edu.cn.

Abstract

Antibiotic-resistant *Serratia marcescens* (*Sm*) is known to cause bloodstream infections, pneumonia, etc. The nod-like receptor family, pyrin domain-containing 3 (NLRP3), has been implicated in various lung infections. Yet, its role in *Sm*-induced pneumonia was not well understood. In our study, we discovered that deletion of *Nlrp3* in mice significantly improved *Sm*-induced survival rates, reduced bacterial loads in the lungs, bronchoalveolar lavage fluid (BALF), and bloodstream, and mitigated the severity of acute lung injury (ALI) compared to wild-type (*WT*) mice. Mechanistically, we observed that 24 hours post-*Sm* infection, NLRP3 inflammasome activation occurred, leading to gasdermin D NH2-terminal (GSDMD-NT)-induced pyroptosis in macrophages and IL-1β secretion. The

NLRP3 or NLRP3 inflammasome influenced the expression PD-L1 and PD-1, as well as the count of PD-L1 or PD-1-expressing macrophages, alveolar macrophages, interstitial macrophages, PD-L1-expressing neutrophils, and the count of macrophage receptors with collagenous structure (MARCO)-expressing macrophages, particularly $MARCO^+$ alveolar macrophages. The frequency of $MARCO^+$ alveolar macrophages, PD-1 expression, particularly $PD\text{-}1^+$ interstitial macrophages were negatively or positively correlated with the *Sm* load, respectively. Additionally, IL-1β levels in BALF correlated with three features of acute lung injury: histologic score, protein concentration and neutrophil count in BALF. Consequently, our findings suggest that *Nlrp3* deletion offers protection agaisnt acute *Sm* pneumonia in mice by inhibiting inflammasome activation and reducing *Sm* infection-induced PD-L1/PD-1 or MARCO expression, particularly in macrophages. This highlights potential therapeutic targets for *Sm* and other gram-negative bacteria-induced acute pneumonia.

Keywords: *Serratia marcescens*; acute lung injury; NLRP3 inflammasome; PD-L1/PD-1; pyroptosis; macrophage receptor with collagenous structure

1. Introduction

Serratia marcescens (*Sm*), a facultatively anaerobic, rod-shaped, gram-negative bacterium within the *Enterobacteriaceae* family, has been identified as one of the antibiotic-resistant priority pathogens by the World Health Organization in 2017 [1]. This pathogen is notably prevalent in nosocomial infections, particularly affecting severely immunocompromised or critically ill patients in intensive care units, especially in neonatal settings. The most common site of *Sm* infection is the bloodstream, followed by the respiratory and the gastrointestinal tracts, often exhibiting multi-resistance [1-3]. González-Juarbe et al [4] developed a murine model to stimulate *Sm* pneumonia, accurately reflecting the clinical aspects of the human illness. The study underscored the crucial roles of neutrophils in the host's defense against this infection. Furthermore, the pore-forming toxin produced by *Sm* was found to induce necroptosis in mouse lung epithelial cells, as well as in the *in vitro* cultured alveolar macrophage cell line MHS and bone marrow-derived macrophage (BMDM) [5, 6].

The nod-like receptor family, pyrin domain-containing 3 (NLRP3) inflammasome, is a

key element of the innate immune system, acting as an innitial defense against pathogens. It is composed of NLRP3, apoptosis-associated speck-like protein containing a carboxy-terminal CARD (ASC), and caspase 1 (Casp1) or noncanonical caspase 11 (Casp11). This complex orchestrates the activation of Casp1 and Casp11, triggering the secretion of proinflammatory cytokines IL-1β/IL-18 and initiating pyroptosis via gasdermin D NH2-terminal (GSDMD-NT) aggregation in the cell membrane in response to microbial infection and cellular damage [7-9]. The function of NLRP3 during bacterial infection can be dual, providing protection or causing harm due to excessive inflammation and cell death, depending on the nature of the pathogen and host cell [7-10]. BMDM from *Nlrp3* or *ASC* knockout mice exhibited partial protection against *Sm* infection and exposure to recombinant pneumolysin, a pore-forming toxin [4]. However, the full understanding of NLRP3 in *Sm*-induced pneumonia remains elusive. Conducting *in vivo* studies using *Nlrp3* deletion mice are crucial to unravel the exact functions and mechanisms of NLRP3 in this specific context.

Immune checkpoints, including programmed death ligand-1 (PD-L1) or its receptor (PD-1), play a crucial regulatory role in modulating both innate and acquired immune responses. The PD-L1/PD-1 pathway has been extensively studied in several bacterial diseases and sepsis, with research spanning both preclinical and clinical studies [11-13]. PD-L1 is expressed by diverse cell types, notably macrophages and neutrophils. The presence of PD-L1-expressing neutrophils and PD-1-positive macrophages has been linked to a reduced bacteria burden [13-18]. Furthermore, multi-omics data analysis from the TCGA database reveals a significant correlation between NLRP3 overexpression and increased levels of PD-1 and PD-L1 across various cancers [19]. The inhibition of NLRP3 inflammasome activation using MCC950 has been shown to significantly reduce the numbers of exhausted PD-1^+ T cells [20]. Additionally, *Nlrp3* deletion has been found to alleviate neutrophil tumor infiltration, thereby markedly enhancing the effectiveness of anti-PD-1 antibody immunotherapy [21]. Elevated IL-1β levels, resulting from NLRP3 inflammasome activation, have been correlate with increased PD-L1 and PD-1 expression, which in turn impacts the prognosis of certain cancers [22-25]. These findings suggested that NLRP3 and the NLRP3 inflammasome may regulate PD-L1/PD-1 pathway via IL-1β.

Our research explores the interrelationship between NLRP3, PD-L1/PD-1 expression

including the frequency of PD-L1/PD-1 expressing cells, and immune responses during acute *Sm* pneumonia. This investigation aims to lay the groundwork for identifying novel therapeutic targets for multi-resistant *Sm* or even other gram-negative microbe infection.

2. Materials and methods

2.1. Cell line and reagents

The human type 2 alveolar epithelial cell line A549 was kindly provided by Prof Tao Peng from the Sino-French Hoffmann Institute, and the mouse macrophage cell line J774A.1 was generously shared by Zhong-Jin Yang from the College of Pharmacy at Guangzhou Medical University. For our experiments, we utilized Caspase-Glo 1/11 Inflammasome Assay kits (G9951 and G9952) obtained from Promega. Various other reagents were employed, including the Hematoxylin-eosin (HE) staining kit (Baso, BA-4025), Bio-Plex Pro-Mouse Group I Cytokine 23-plex assay (M60009RDPD, Bio-Rad, Hercules, California, USA), antibodies against mouse IL-1β (#12242, CST), GSDMD (ab219800, Abcam, Cambridge, MA), PD-L1 (ab233482, Abcam, Cambridge, MA), PD-1 (#84651, CST) and GAPDH (ab181603, Abcam, Cambridge, MA). Additionally, Goat anti-rabbit IgG (H+L), HRP conjugate (Proteinch, SA00001-2) was used for immunohistochemistry staining (IHC) and western blotting (WB). We also employed Compound 4a (566914-00-9, MCE, USA), an IL-1 receptor antagonist (IL-1Ra) to inhibit IL-1α/1β receptor-mediated responses [26].

2.2. Mice, ethics statement, and treatment

Nlrp3 knockout mice (*Nlrp3*$^{-/-}$) were acquired from Jackson Laboratory (JAX: 000664), USA. Wild-type C57BL/6 mice (*WT*) were sourced from Beijing Biotechnology Co Ltd, China. We housed the mice in specific-pathogen-free (SPF) conditions and used them at the age of 6-8 weeks. Each mouse received an intra-oropharyngeal inoculation with a specific dose of *Sm*. All animal experiments were performed following the guidelines and with the approval of the Institutional Animal Care and Use Committee at South China Agricultural University (authorization no: 2019c013).

2.3. Bacterial strain and growth conditions

The *Sm* strain isolated from *Drosophila* (*Db11*) and the clinically isolated strain *RM26626* were both maintained by the Dominique Ferrandon/Zi Li's group at the Sino-

French Hoffmann Institute of Guangzhou Medical University. Additionally, another clinically isolated *Sm* strain was generously provided by Dan-Hong Su from the State Key Lab of Respiratory Disease (*SKLRD*) at Guangzhou Medical University. For culturing, the *Sm* strains were grown on Luria-Bertani (LB) agar plates, incubated overnight at 30°C. To prepare the inocula, bacteria were diluted in sterile phosphate-buffered saline (PBS) to the required concentration (50μl volume per inoculum). The count of colony-forming units (cfu) present in each inoculum was verified at the time of infection through serial dilution and plating on agar plates, followed by extrapolation based on the number of colonies.

2.4. Hematoxylin and eosin (H&E) staining and immunohistochemistry staining (IHC)

Paraffin-embedded lung tissue sections were utilized for IHC or H&E staining to assess the extent of lung injury. The semi-quantification and histologic scores were conducted based on established criteria [27, 28], with the scoring system detailed in Table S1. We evaluated the expression levels and subcellular location of IL-1β, GSDMD-NT, PD-L1, or PD-1 in the lung tissues of the designated mice using IHC. The images of these tissues were captured using an optical microscope (Olympus, Japan). Their semi-quantitative analysis was performed using Image J software and the results were presented as H scores [29].

2.5. RNA isolation and quantitative PCR

Total RNA was extracted from fresh lung tissues using a Trizol reagent. Following the manufacturer's instructions, cDNA synthesis was perfoumed and sebsequently amplified by reverse transcription quantitative real-time PCR (RT-qPCR). The primer sequences utilized in this study are listed in Table S2. The mRNA expression levels of individual genes were normalized to GAPDH and calculated using the $2^{-\Delta\Delta Ct}$ method for data analysis.

2.6. Analysis of BALF

After performing a tracheotomy, lungs were lavaged thrice with 0.5 mL of PBS each time to collect BALF. The BALF was then centrifuged and resuspended in 0.5ml PBS. The total cell count was determined using the Cellometer Slide Chamber (Nexcelom Biosciences), and a single cell suspension was prepared for flow cytometry. Total protein levels in the BALF were quantified using a BCA assay kit (Guangzhou Dingguo Biology). The activities of Casp1 and Casp11 in the BALF supernatant were detected using the Caspase-Glo 1 Inflammasome Assay kit. LDH in BALF (OD_{490}) was measured according

to the CytoTox96 non-radioactive cytotoxicity assay kit (G1780, Promega). Furthermore, 23 cytokines in the BALF supernatant, including 4 proinflammatory cytokines [IL-1α, IL-1β, IL-6 and tumor necrosis factor α (TNF-α)], chemokines for granulocyte and monocyte –[Eotaxin (CCL11), monocyte chemoattractant protein 1 (MCP-1), macrophage inflammatory protein-(MIP)-1α, MIP-1β and Regulated on Activation, Normal T Expressed and Secreted (RANTES, or CCL5)], colony-stimulating cytokines [IL-3, granulocyte colony-stimulating factor (G-CSF) and granulocyte-macrophage colony-stimulating factor (GM-CSF)], and activatory and differentiating cytokines for innate lymphoid cells or T cell subsets [IL-2, IL-12(p40), IL-12(p70), interferon-gamma (IFN-γ), IL-4, IL-5, KC, IL-9, IL-10, IL-13 and IL-17A], were analyzed using the Bio-Plex Pro-Mouse Group I Cytokine 23-plex assay (M60009RDPD, Bio-Rad, Hercules, California, USA) on a BioRad Bio-Plex 200 system, MAGPIX Multiplex Reader (Bio-Rad Laboratories, Life Science Group 2000, Hercules, CA, USA).

2.7. Preparation of single-cell suspensions in mice lung or BALF

After anesthesia, peripheral blood was collected from the mice via retro-orbital bleeding. Subsequently, sterile normal saline (NS) was injected into the left ventricle to clear blood from the organs. Following the collection of BALF, mice lungs were excised, finely separated using forceps, and then digested in a solution of 3mg/mL collagenase Type II (Gibico, 17101015) and 3mg/mL DNase I (Roche, 10104159001) for 1 hour at 37℃. The digested lung cells and BALF cells were then passed through a 100μm cell strainer. Red blood cells in the single-cell suspensions from the lungs and BALF were lysed using ammonium chloride (NH4Cl) for 10 minutes. The resulting cell suspensions was treatd with a Fc block antibody (BD, clone 2.4G2), followed by a 20-minute incubation with the BV510 Fixable Viability Kit (65-0866-14, Biolegend). Finally, the cells were resuspended in complete RPMI 1640 medium containing 10% fetal bovine serum (FBS) at a concentration of 2–3 × 10^6 cells/ml.

2.8. Cell surface staining and flow cytometry analysis

The upper layer of the cell suspensions was used for cell surface marker staining , with specific antibodies detailed in Table S3. These stained cells were then analyzed through flow cytometry (FACS) using a CytoFLEX system (Beckman Coulter), and the data were processed with FlowJo software. In this analysis, neutrophils (Neu) were

identified as $CD45^+CD11b^+Ly6G^+$, macrophages (MA) as $CD45^+Ly6G^-F4/80^+$, monocytes (Mon) as $CD45^+Ly6G^-CD11b^+Ly6C^+$, alveolar macrophages (AM) as $CD45^+Ly6G^-F4/80^+$ $CD11b^-$, and interstitial macrophage (Int-MA) as $CD45^+Ly6G^-F4/80^+CD11b^+$.

2.9. Western blotting (WB)

Protein were extracted from the specified cell lysate using radio-immunoprecipitation assay (RIPA) buffer. Equal amounts of these proteins were then seperated on 10% SDS-polyacrylamide gels and subsequently transferred onto PVDF membranes. After incubation with primary antibodies (GSDMD, GAPDH, PD-1, PD-L1) followed by secondary antibodies, the target proteins were visualized using an enhanced chemiluminescence (ECL) reagent, in accordance with the manufacturer's protocol.

2.10. RNA interference (RNAi) Assay

Small interfering RNA (siRNA) sequences targeting mouse GAPDH (siGAPDH), NLRP3 (siNLRP3), GSDMD (siGSDMD), along with a negative control sequence (siNC), were synthesized by Beijing Tsingke Biotech Co., Ltd. The sequence of 3 siRNAs of NLRP3 was: 5'- GGATCTTTGCTGCGATCAA-3', 5'- CGTGAAGGTCCTACTAGAA-3', 5'- GCAGGTTCTACTCTATCAA-3', and siGSDMD was: 5'- GTTCCTATTGTCAAGTCTA-3'. J774A.1 cells were transfected with these siRNAs using ScreenFect siRNA (Cat no: 295-75003, FUJIFILM, Tokyo, Japan) for 36 h, following the manufacturer's protocol. For siRNA transfection, cells treated with 66.67nM of either siNLRP3, siGSDMD or siNC. Normal control group (NC), in contrast, were treated only with ScreenFect siRNA reagents without any siRNA.

2.11. Statistical analysis

Data are presented as means ± standard error of the mean (SEM) or standard deviation (SD). Comparative analyses were performed using a two-tailed Student's *t*-test or analysis of variance (ANOVA). Kaplan–Meier curves and the log-rank test were employed to analyze differences in overall survival between two groups. Descriptive statistics and correlation analyses were performed with GraphPad Prism version 8.0.

3. Results

3.1. NLRP3 genetic deletion significantly improved mice survival and lowered bacterial load.

High doses (5 X 10^7cfu) of clinically isolated strains, including *RM66262* and *SKLRD,* resulted in 100% mouse mortality within 24 hours. In contrast, mice infected with the strain isolated from *Drosophila-Db11* infection experienced a lower mortality rate, with death occurring within 63 hours (n=7, $P<0.01$) (Figure 1A). Therefore, *Db11* exhibited lower virulence compared to clinical isolates, making it also suitable for constructing a mouse *Sm* pneumonia model. To assess the progression of *Db11* pneumonia over time, we tested LDH release in BALF at OD_{490} using a CytoTox96 non-radioactive cytotoxicity assay kit. BALF LDH was significantly increased at 12 hours (12 h) and 24 h post-*Db11* infection, while no significant changes were observed at 3 h, 6 h, 2 days (2 d), 4 d, and 8 d post-infection (Figure 1B). Consistently, H&E staining showed a gradual enlargement of the area of immune cell infiltration from 3 to 24 h, followed by progressive recovery at 2, 4, and 8 d post-*Db11* infection (Figure 1C).

To detect the role of NLRP3 in *Sm*-induced mice pneumonia, we utilized *Nlrp3* deletion mice. Deletion mice exhibited significantly higher survival percentage than *WT* mice during lethal doses of *Db11* (5.5×10^7cfu) infection (Figure 1D, $P=0.042$). Additionally, *Nlrp3*$^{-/-}$ mice demonstrated significantly reduced bacteria loads in the lung, BALF, and blood compared to *WT* mice after a sub-lethal dose of *Db11* infection (5×10^6cfu) for 24 hours (Figure 1E-1G).

3.2. Nlrp3 knockout alleviated the severity of acute lung injury induced by 24 h of Sm infection.

To further assess the involvement of NLRP3 in acute *Sm* pneumonia, we tested features of acute lung injury based on the criteria outlined in An Official American Thoracic Society Workshop Report from 2011 and 2022 [27, 28]. The evidence of tissue injury was evaluated by H&E staining and semi-quantified with a modified scoring system (Table S1). Changes in the alveolar-capillary barrier were determined by quantifying BALF total protein concentration using a BCA protein assay kit. The severity of the inflammatory response was assessed by measuring cytokines or chemokines in BALF via Bio-Plex Pro-Mouse Group I Cytokine 23-plex assay and counting neutrophils and inflammatory macrophages in the lung or BALF using flow cytometry.

After 24h of *Db11* infection, *WT* mice lungs exhibited a significantly elevated histologic score, characterized by the presence of numerous neutrophils within alveoli and

interstitial spaces compared to *Nlrp3*$^{-/-}$ mice and non-infection mice (red arrows-neutrophils, Figure 2A). The concentrations and heatmap of 23 cytokines' levels in BALF were shown in Table S4 and Figure 3B, respectively. Among them, the levels of four pro-inflammatory cytokines, namely IL-1α, IL-1β, IL-6, and TNF-α were significantly increased in *Db11*-infected *WT* mice compared to non-infected mice, while *Nlrp3* deletion significantly decreased these levels (Table S4, Figure 3B, 3C). Granulocyte and monocyte/macrophage chemokines such as Eotaxin, KC, RANTES, and colony-stimulating factors such as IL-3 and GM-CSF followed a similar trend as these four pro-inflammatory cytokines. IL-12(p40) significantly increased during *Sm* infection and further rose due to *Nlrp3* deletion. MCP-1, MIP-1α, MIP-1β, G-CSF, and IL-4 were significantly induced by *Sm* infection, whereas IL-2 and IFN-γ levels decreased significantly. Compared to infected *WT* mice, IL-13 was not induced by infection but significantly decreased by *Nlrp3* deletion (Table S4, Figure 3B).

The inflammatory response induces lung barrier damage, reflected in a heightened BALF total protein concentration. In infected *WT* mice, the BALF total protein level was significantly elevated compared to non-infection, and *Nlrp3* deletion mitigated this increase (Figure 3D). In comparison to non-infection, the frequency of neutrophils (Neu) of CD45^{+} cells in the lung and BALF markedly increased due to *Db11* infection, while *Nlrp3* deletion slightly but significantly decreased this frequency (Figure 3E, 3F). Briefly, *Db11* infection led to acute lung injury which was alleviated by *Nlrp3* deletion.

3.3. NLRP3 inflammasome in macrophage was activated during acute Db11 infection, and Nlrp3 knockout recovered the count of macrophages and their subsets.

Given the absence of in vivo research on the implication of NLRP3 inflammasome in acute *Db11* infection, we checked the existence of the triggering signal of its activation-the transcription level of *Nlrp3*, *Casp1*, *Casp11,* and *Il1b, Il18* in the lung of *WT* mice. In 3 h of *Db11* infection, they were induced but statistically insignificant due to high variation among individual samples. However, at 12 h and 24 h of infection, *Nlrp3*, *Casp11,* and *Il1b* were significantly upregulated, while *Casp1* was significantly elevated only at 12 h, not at 24 h, and *Il18* remained insignificant (Figure 3A). These suggest that IL-1β but not IL-18 as the inflammasome activation marker, is involved in acute *Db11* pneumonia. Casp1 activity in BALF significantly decreased at 3 h of *Db11* infection (P<0.05) but significantly

increased at 12 h and 24 h (P<0.05). Casp11 activity in BALF significantly increased at 3 and 12 h of infection (P<0.05) and slightly increased at 24 h (Figure 3B). Through IHC staining, we found that IL-1β was predominantly located in cells around the alveoli and infiltrating immune cells around the bronchial (Figure 3C, blue arrow). Hence, the NLRP3 inflammasome was significantly activated at 12 h and 24 h of acute *Db11* infection-induced mice pneumonia.

High level of GSDMD cleavage or aggregated GSDMD-NT-induced cell pyroptosis and IL-1β because of Casp1 and Casp11 activation marked as NLRP3 inflammasome activation. González-Juarbe et al. [6] reported that F4/80^{+} cells around alveoli disappeared strikingly during 48h of *Sm* infection-induced pneumonia, and NLRP3 was involved in *Sm* infection-induced necroptosis of alveolar macrophage cell line MHS and BMDM. Herein, the cleavage band of the full length of GSDMD (GSDMD-FL) into GSDMD-NT in *in vitro* culturing type 2 alveolar epithelial cell line A549 was not detectable (Figure 3D, left) but was shown in mouse macrophage line J774A.1 with 12 h and 24 h of *Sm* infection (Figure 3D, right) by WB. IL-1β level in BALF was increased during *Sm* infection and was decreased because of *Nlrp3* deletion, as shown in Figure 2B, 2C. The activity of Casp1 showed the same tendency as IL-1β (Figure 3E). Furthermore, GSDMD was significantly downregulated in *Sm*-infected *Nlrp3*$^{-/-}$ mice lungs compared to *WT* mice. In *Sm*-infected WT mice's lungs, GSDMD is located in the infiltrated immune cells (Figure 3F). *Db11* infection significantly increased the frequency of interstitial macrophages (Int-MA) while significantly decreasing the count of macrophages (MA), especially alveolar macrophages (AM), compared to *Nlrp3*$^{-/-}$ mice and non-infection mice (Figure 3G). Through correlation analysis, the level of lung GSDMD, BALF IL-1β level had a significant negative correlation with the frequency of lung MA and AM, while they had a significant positive correlation with lung Int-MA (Figure 3H-3J). Therefore, 24 h of *Db11* infection triggered NLRP3 inflammasome activation in macrophages and then GSDMD-NT-induced pyroptosis of alveolar macrophages and IL-1β secretion.

3.4. Inhibition of NLRP3 inflammasome activation decreased the expression of PD-1 and PD-L1, and the count of PD-L1 and PD-1 positive macrophages during 24 h of Db11 infection.

The PD-L1/PD-1 pathway has been addressed in various bacterial diseases and sepsis

[11-13]. NLRP3 inflammasome activation has been associated with poor prognosis in some cancers due to its correlation with high PD-L1 and PD-1 expression [22-25]. Through IHC staining and semi-quantifying analysis, we found that *Nlrp3* deletion significantly decreased the expression levels of PD-L1 and PD-1 in the lungs of *Sm*-infected mice (Figure 4A and 4B), a finding further confirmed by flow cytometry. *Nlrp3* deletion significantly lowered the frequency of PD-1$^+$ cells and PD-L1$^+$ cells of live cells in the lung during *Db11* infection (Figure 4C and 4D).

In vitro, using the J77A.1 macrophage cell line, we investigated the interplay between NLRP3, GSDMD-NT, and IL-1β (indicators of NLRP3 inflammasome activation) and PD-L1 and PD-1 during a 6-hour *Db11* infection. Among three siRNAs targeting NLRP3, siRNA no1 and no3 demonstrated greater efficacy in reducing NLRP3 expression. In response to *Db11* infection, we observed an increase in the expression of NLRP3 and PD-1, while PD-L1 was slightly increased (Figure 5A-5C). Moreover, the expression levels of PD-1 were suppressed following transfection with NLRP3 and GSDMD siRNA (Figure 5A, 5B) and by pre-treatment with IL-1Ra, while PD-L1 expression was suppressed by siGSDMD and IL-1Ra but not siNLRP3 (Figure 5C). *In vivo*, through flow cytometry, we found a significant increase in the frequency of PD-L1$^+$ macrophages (PD-L1$^+$MA) and PD-L1$^+$ interstitial macrophages (PD-L1$^+$Int-MA) in the total macrophage population n *Db11*-infected *WT* mice, compared to non-infected controls (Figure 5D, 5E). This increase was also notable in corresponding PD-1$^+$ macrophage subpopulations (Figure 5F, 5G). Intriguingly, NLRP3 genetic deletion markedly reduced the percentages of these *Db11*-induced macrophage populations (Figure 5D-5G). While *Db11* infection didn't significantly alter the frequency of PD-L1$^+$ and PD-1$^+$ alveolar macrophages (PD-1$^+$AM) within total MA in *WT* mice, NLRP3 genetic deletion led to a significant increase in the percentages of PD-1$^+$AM within total MA (Figure 5E, 5G).

In *Db11*-infected *WT* mice, we noted a significant rise in the frequency of PD-L1$^+$ neutrophils (PD-L1$^+$Neu) and PD1$^+$ neutrophils (PD1$^+$Neu) among the total neutrophil population, in comparison to non-infected controls. This was discernible in the significantly lower percentage of PD-L1$^+$Neu within the total neutrophil population after NLRP3 genetic deletion (Figures S1A, S1B). Given the crucial role of resident memory T cells in barrier immunity, as well as regulatory T cells (Treg) and γδT cells in the innate

immune response, we proceeded to analyze alterations in these T cell subsets and their PD-1 expression during *Nlrp3* knockout and after a 24-hour *Db11* infection. We discovered that *Db11* infection substantially increased the numbers of $CD4^+$ T cells (Th), $Foxp3^+$ T cells (Treg), and $\gamma\delta TCR^+$ T cells ($\gamma\delta$T), but not $CD8^+$ T cells (cytotoxic T lymphocyte, CTL). Post *Nlrp3* knockout, we observed a significant increase in the counts of CTL while decrease in Treg cells, while the numbers of Th and $\gamma\delta$T cells remained relatively unchanged (Figure S2B). Additionally, the frequency of PD-1 expression in Th, Treg, and $\gamma\delta$T cells out of their respective parent T cell populations was elevated by a 24-hour *Db11* infection. Conversely, PD-1 expression in Th, CTL, or Treg cells showed a significant decline following *Nlrp3* deletion (Figure S2C).

In summary, NLRP3 genetic knockout significantly reduced PD-L1 expression in macrophages, neutrophils or Treg cells, as well as PD-1 expression in macrophages, Th, CTL and Treg cells. Our findings suggested that NLRP3 modulated PD-1 and PD-L1 expression in macrophages through inflammasome activation-triggered GSDMD-NT and IL-1β production during *Db11* infection.

3.5. NLRP3-controlled acute Sm pneumonia was correlated with the frequency of PD-1 expression or MARCO in MA, and with IL-1β levels in the lung.

Neutrophils play a crucial role in *Sm* clearance [4]. In our study, despite the higher frequencies of Neu and Int-MA in *WT* mice compared to *Nlrp3*$^{-/-}$ mice (Figure 2E, 3G), the bacterial load in the lung of *WT* mice was higher than *Nlrp3*$^{-/-}$. Moreover, there was no significant correlation between *Sm* load and the count of neutrophils in the lung and in BALF (Figure S3A), as well as the count of MA or their subsets (Figure S3B) or T cell subsets (Figure S3C) in the lung. PD-$L1^+$ and PD-1^+ neutrophils and macrophages, monocytes have been linked to infection susceptibility [11-18, 30]. Hence, we analyzed the correlation of PD-1, PD-L1 and the frequency of these molecules in cell populations with *Sm* load. As shown in Figure 6A, 6B, only the frequency of PD-1^+ cells of live cells, PD-1 expressing MA and Int-MA of MA were positively correlated with lung *Sm* load (R^2>0.5, P<0.05). No significant correlation was found with the count of PD-$L1^+$ cells (Figure S4A), PD-$L1^+$ MA and their subsets (Figure S4B), PD-1^+AM (Figure 6B, middle panel), PD-1 or PD-$L1^+$ neutrophils (Figure S4C), and PD-1 expressing T cell subsets (Figure S4E).

MARCO belongs to the class A scavenger receptor molecules, playing a crucial role

in eliminating microbes through un-opsonised binding and activating phagocytosis [31, 32]. Autoantibodies against MARCO in macrophages in eosinophilic asthma airways have been shown to impede effective host defenses against bacterial infection [33]. Our results revealed that in the BALF of *Nlrp3* deleted mice with *Db11* infection, there was a significantly higher frequency of $MARCO^+$ macrophage, predominantly $MARCO^+$AM in macrophages, compared to infected *WT* mice (Figure 6C-6E). Correlation analysis demonstrated a strong negative correlation between the frequency of both $MARCO^+$MA and $MARCO^+$AM with bacterial load in BALF (Figure 6F). Thus, the reduced PD-1 expression in lung macrophages and the induced MARCO on the surface of lung macrophages, especially alveolar macrophages, might explain the lower bacterial load in *Nlrp3* deleted mice lungs. The mechanisms through which NLRP3 affects PD-1 and MARCO expression warrant further investigation.

Additionally, BALF IL-1β level (Figure 6G) but not Casp1 activity in BALF (Figure S5A) or GSDMD expression levels in the lung (Figure S5B) significantly correlated with three features of acute lung injury, including histologic score, protein concentration in BALF, and the amount of neutrophils in BALF. BALF IL-1β level also significantly correlated with the frequency of $MARCO^+$MA in MA (Figure 6H). PD-1 or PD-L1 expression or their expression in macrophages or their subsets showed no significant correlation with the frequency of $MARCO^+$AM in MA (Figure S6). Therefore, acute *Db11* infection induced acute lung injury and subsequent pyroptosis of macrophages, especially alveolar macrophages, through NLRP3 inflammasome activation. In the lungs of *Sm* infected *Nlrp3*$^{-/-}$ mice, with inhibited NLRP3 inflammasome activation, the AM count was restored, and acute lung injury was alleviated.

4. Discussion

This study reveals that acute *Sm* infection triggers NLRP3 inflammasome activation, leading to acute lung injury and an increased bacterial load in the lung and bloodstream. A key discovery is that *Nlrp3* deletion, in comparison to *WT* mice, provides protection against acute *Sm* pneumonia, as evidenced by a significantly reduced severity of acute lung injury, diminished levels of various inflammatory cytokines/chemokines, and a decreased bacterial load. The mechanism behind this protection involves the suppression of PD-1 and PD-L1 expression during acute *Sm* infection due to *Nlrp3* deletion. Notably, there is a

404 significantly reduction in PD-L1^{+} cells (MA, Int-MA, Neu), and PD-1^{+} MA, Int-MA in the
405 lungs of *Nlrp3*$^{-/-}$ mice infected with *Sm* for 24 hours. Conversely, there is an increasing in
406 MARCO^{+} macrophages in BALF compared to infected *WT* mice. This increase in
407 MARCO^{+} macrophages (alveolar macrophages) in BALF, along with lower PD-1^{+}
408 expression or PD-1^{+} macrophages (interstitial macrophages) in the lung, correlates with
409 decreased *Sm* load or enhanced *Sm* clearance. In addition, the study finds a significant
410 correlation between GSDMD levels in the lung with macrophage counts, including AM
411 and Int-MA. BALF IL-1β levels correlate strongly with features of acute lung injury and
412 with MARCO^{+}MA. Furthermore, interfering with GSDMD transcription or inhibiting IL-
413 1 signaling in *Sm*-infected macrophage reduces PD-L1 and PD-1 expression. Thus, *Nlrp3*
414 deletion shields against acute *Sm* pneumonia by inhibiting NLRP3 inflammasome
415 activation, which lowers GSDMD and IL-1β levels. This leads to reduced PD-L1 and PD-
416 1 expression, especially in macrophages. This investigation is groundbreaking the role of
417 NLRP3, NLRP3 inflammasome, PD-L1 and PD-L1 expression, particularly in
418 macrophages, and the involvement of MARCO^{+} macrophages in combating *Sm* pneumonia.
419 Canonical NLRP3 inflammasome activation in response to gram-negative bacteria
420 infection comprises two signals: Signal 1, initiated by LPS (released from the bacterial cell
421 wall) /TLR4, triggers NF-κB signaling. Signal 2 involves pore-forming toxin-mediated
422 Ca^{2+} influx and K^{+} efflux, exemplified by nigericin. LPS and pore-forming toxin from *Sm*
423 potentially trigger and activate NLRP3 inflammasome. According to the results from
424 González-Juarbe N et al. [6], F4/80^{+} alveolar macrophages around alveoli in BALB/C mice
425 with 48 h post-*Sm* infection nearly completely disappeared through immunofluorescence
426 staining. Necroptosis was identified as the major cell death pathway in *in vitro* cultured
427 alveolar macrophage cell line MHS and BMDM during *Sm* infection or recombinant pore-
428 forming toxin stimulation. BMDM from *Nlrp3*$^{-/-}$ mice exhibited a protective trend against
429 *Sm* infection. Our results also indicated the protective role of NLRP3 against *Sm* infection
430 using *Nlrp3*$^{-/-}$ mice. After confirming the induction of GSDMD-NT in J774A.1 cells during
431 acute *Sm* infection, we found a lowered expression level of GSDMD-NT within *Nlrp3*$^{-/-}$
432 mice lung during *Sm* infection. Therefore, Both NLPR3-regulated GSDMD-mediated
433 pyroptosis and p-MLKL-mediated necroptosis might contribute the death of alveolar
434 macrophages and influence the severity of *Sm* pneumonia.

PD-1^{+} neutrophils, macrophages, and monocytes have been associated with increased susceptibility to infection [11-18, 30]. PD1^{+} tumor-associated macrophages exhibit reduced phagocytosis [34] and PD-1-mediated anti-inflammatory M2 macrophage polarization [35]. Ding et al. demonstrated that NLRP3 overexpression promotes immune escape in cancers by upregulating immune checkpoints, including PD-L1 and PD-1 [19]. IL-1β has been correlated with poor prognosis and PD-1 expression in patients with lung adenocarcinoma [22]. A high concentration of IL-1β has the potential to induce PD-L1 expression [12, 14, 22, 36]. NF-κB directly induces transcription of the PD-L1 gene by binding to its promoter or indirectly regulates PD-L1 expression post-transcriptionally in cancer [37]. LPS/TLR4 signaling, IL-1β/IL-1β receptor signaling might activate the NF-κB pathway since LPS, given that LPS from *Sm*'s cell wall could be released due to the immune response, and IL-1β concentration was significantly elevated in the BLAF of *Sm*-infected mice. High concentration of IL-6, TNF-α, IL-2, IL-4, IL-10, IL-12, IFN-γ, IL-17, TGF-β and GM-CSF have been reported to induce PD-L1 expression [12, 14, 22, 36]. *Sm* induced significantly high concentrations of IL-1β, IL-6, IL-12(p40), TNF-α and GM-CSF in the BALF of *WT* mice. In contrast, in the BALF of *Sm* infected *Nlrp3*$^{-/-}$ mice, the concentrations of IL-1β, IL-4, IL-6, TNF-α, and GM-CSF decreased, while IL-12(p40) significantly increased. Therefore, IL-1β itself or through the regulation of IL-6, GM-CSF might contribute to the frequency of PD-L1 and PD-1 expressing macrophages in the lungs of *Sm*-infected *WT* or *Nlrp3*$^{-/-}$ mice within 24 hours. Moreover, we demonstrated that GSDMD-NT production plays a role in controlling PD-L1 and PD-1 expression in macrophages.

MARCO plays a crucial role in microbial clearance through un-opsonized binding and activating phagocytosis [31, 32]. Deletion of *Nlrp3* provides protection against polymicrobial sepsis and enhances MARCO expression in peritoneal cells [38]. We consistently observed an induction of MARCO^{+} macrophages (alveolar macrophages) in the BALF of *Nlrp3* deletion mice during 24 h of *Sm* infection, and its frequency positively correlated with *Sm* clearance. In the absence of MARCO, alveolar macrophages exhibit a greater NLRP3 inflammasome activation and increased susceptibility to silica [39]. The relationship between MARCO and NLRP3 may constitute a reverse feedback loop. Since *Sm* load was correlated with PD-1 and MARCO expression in different macrophage subsets (interstitial macrophage and alveolar macrophage, respectively) during NLRP3

knockout.

Ding L et al. concluded that targeting $MARCO^+$ tumor-associated macrophages can significantly improve anti-PD-L1 resistance in liver cancer [40]. Therefore, PD-1 and MARCO expression macrophages might play parallel roles in *Sm* clearance. The specific molecular mechanisms by which NLRP3 or the NLRP3 inflammasome regulate the expression of PD-L1, PD-1 or MARCO remain to be further elucidated. Additionally, the work of González-Juarbe et al. has highlighted the crucial role of neutrophils in clearing *Sm*, as evidenced by the administration of Ly6G antibody in mice (n=8 or 9) [4]. In line with this, our findings suggest a nearly significant correlation between the *Sm* load and several cellular counts. Specifically, there is a notable correlation with count of neutrophils in the lungs (R^2=0.55, *P*=0.057) or in the BALF (R^2=0.41, *P*=0.065), as well as with the count of Treg cells (R^2=0.32, *P*=0.086) and PD-1^+ Treg cells (R^2=0.31, *P*=0.098). It is conceivable that increasing the sample size, which was 7 or 8 mice in our study, might lead to these correlations achieving statistical significance.

On the other hand, we concluded that acute lung injury in mice was induced after 24 h of *Sm* infection, and the severity of this injury was significantly reduced with *Nlrp3* deletion. This finding aligns with reported studies indicating the involvement of NLRP3 or NLRP3 inflammasome in acute lung injury induced by LPS, COVID-19 infection, and *pseudomonas aeruginosa* infection [41-46]. Therefore, targeting NLRP3 and NLRP3 inflammasome could be a promising therapeutic approach for various causative factors in acute lung injury or pneumonia.

5. Conclusions

The deletion of *Nlrp3* markedly ameliorated acute pneumonia triggered by *Sm* infection within 24 hours. This reduction in severity was attribute to the suppression of NLRP3 inflammasome activation. This suppression led to a decrease in inflammatory cytokines and a restoration of macrophage populations, particularly in alveolar macrophages, due to reduced GSDMD-NT-induced pyroptosis of these cells. Additionally, the decreased expression of PD-1 in interstitial macrophages, combined with an increase in MARCO expression on alveolar macrophages, significantly enhanced the host's bacterial clearance. Both IL-1β and GSDMD were crucial in modulating PD-1 and PD-L1 expression in macrophages during *Sm* infection, with IL-1β also closely associated with

the severity of acute lung injury and the prevalence of $MARCO^+$AM. Therefore, targeting elements such as NLRP3, the NLRP3 inflammasome, IL-1β, GSDMD, PD-1, and PD-L1, particularly NLRP3, may offer promising therapeutic approaches for treating multidrug-resistant *Sm* pneumonia and other microbial pneumonias.

Supplementary Materials: Table S1: Lung injury scoring system (H&E staining). Table S2: Primer pairs' sequences of mice genes used in RT-qPCR. Table S3: Anti-mouse antibodies used for flow cytometry. Table S4: The levels of 23 cytokines in BALF of mice from indicated groups. Figure S1: Detection of PD-L1 or PD-1 expression in neutrophils within the lungs of both *Nlrp3*$^{-/-}$ and *WT* mice after *Sm* infection using flow cytometry for analysis. Figure S2: The frequency of various T cell subsets or PD-1 expression within this subsets in the lungs of *Nlrp3*$^{-/-}$ mice and *WT* mice, both with or without *Sm* infection, as determined by by flow cytometry. Figure S3: The correlations between neutrophils or macrophage populations with bacterial load during acute *Sm* pneumonia. Figure S4: The relationships between the frequency of PD-$L1^+$ cells in their respective parent populations, and PD-1^+ neutrophils or T cell subset in the lungs with lung bacterial load. Figure S5: The correlations between Casp1 activity or GSDMD expression levels with three features of acute lung injury. Figure S6：The correlations between the frequency of PD-L1, PD-1 expression cell population and $MARCO^+$MA.

Author Contributions: Z. L. and KF.L. conceived the science and designed the experiments. KY.C., SY.L., and JJ.T. contributed equally to the work. KY.C., SY.L., JJ.T., MK.L., XY.C., and ZP.L. performed the experiments and analyzed the data. D.F. and KF.L. helped to develop the science and interpreted the results. The manuscript was written by Z.L. and JJ.T. and edited by D.F. and Z.L. All authors read and approved the final manuscript.

Funding: This work was supported by 111 Project (No. D18010), the open project program of the state key laboratory of respiratory disease (No. SKLRD-MS-201801), and the Natural Science Foundation of Guangdong province (No. 2023A1515012451).

Institutional Review Board Statement: All experimental procedures followed the National Institute of Health Guidelines for Laboratory Animals and were approved by the Animal Ethics Committee of South China Agricultural University (authorization no: 2019c013).

Informed Consent Statement: Not applicable.

Data Availability Statement: All data generated or analyzed during this study are included in this published article. The original data will be made available on reasonable request.

Acknowledgments: We thank Professor Tao Peng and Zhong-Jin Yang for the cell line, and Professor Dan-Hong Su for the clinical *Sm* strain isolates.

Conflicts of Interest: The authors have declared that no conflict of interest exists.

References

1. Breijyeh Z, Jubeh B, Karaman R: **Resistance of Gram-Negative Bacteria to Current Antibacterial Agents and Approaches to Resolve It**. *Molecules* 2020, **25**(6).
2. Cristina ML, Sartini M, Spagnolo AM: **Serratia marcescens Infections in Neonatal Intensive Care Units (NICUs)**. *International journal of environmental research and public health* 2019, **16**(4).
3. Yayan J, Ghebremedhin B, Rasche K: **Cefepime shows good efficacy and no antibiotic resistance in pneumonia caused by Serratia marcescens and Proteus mirabilis - an observational study**. *BMC pharmacology & toxicology* 2016, **17**:10.
4. González-Juarbe N, Mares CA, Hinojosa CA, Medina JL, Cantwell A, Dube PH, Orihuela CJ, Bergman MA: **Requirement for Serratia marcescens cytolysin in a murine model of hemorrhagic pneumonia**. *Infection and immunity* 2015, **83**(2):614-624.
5. González-Juarbe N, Bradley KM, Shenoy AT, Gilley RP, Reyes LF, Hinojosa CA, Restrepo MI, Dube PH, Bergman MA, Orihuela CJ: **Pore-forming toxin-mediated ion dysregulation leads to death receptor-independent necroptosis of lung epithelial cells during bacterial pneumonia**. *Cell death and differentiation* 2017, **24**(5):917-928.
6. González-Juarbe N, Gilley RP, Hinojosa CA, Bradley KM, Kamei A, Gao G, Dube PH, Bergman MA, Orihuela CJ: **Pore-Forming Toxins Induce Macrophage Necroptosis during Acute Bacterial Pneumonia**. *PLoS pathogens* 2015, **11**(12):e1005337.
7. Hayward JA, Mathur A, Ngo C, Man SM: **Cytosolic Recognition of Microbes and Pathogens: Inflammasomes in Action**. *Microbiology and molecular biology reviews : MMBR* 2018, **82**(4).
8. Paik S, Kim JK, Silwal P, Sasakawa C, Jo EK: **An update on the regulatory mechanisms of NLRP3 inflammasome activation**. *Cellular & molecular immunology* 2021, **18**(5):1141-1160.
9. Tupik JD, Markov Madanick JW, Ivester HM, Allen IC: **Detecting DNA: An Overview of DNA Recognition by Inflammasomes and Protection against Bacterial Respiratory Infections**. *Cells* 2022, **11**(10).

10. Wang Y, Cao C, Zhu Y, Fan H, Liu Q, Liu Y, Chen K, Wu Y, Liang S, Li M *et al*: **TREM2/β-catenin attenuates NLRP3 inflammasome-mediated macrophage pyroptosis to promote bacterial clearance of pyogenic bacteria**. *Cell death & disease* 2022, **13**(9):771.
11. Abers MS, Lionakis MS, Kontoyiannis DP: **Checkpoint Inhibition and Infectious Diseases: A Good Thing?** *Trends in molecular medicine* 2019, **25**(12):1080-1093.
12. Qin W, Hu L, Zhang X, Jiang S, Li J, Zhang Z, Wang X: **The Diverse Function of PD-1/PD-L Pathway Beyond Cancer**. *Frontiers in immunology* 2019, **10**:2298.
13. Patil NK, Guo Y, Luan L, Sherwood ER: **Targeting Immune Cell Checkpoints during Sepsis**. *International journal of molecular sciences* 2017, **18**(11).
14. Thanabalasuriar A, Chiang AJ, Morehouse C, Camara M, Hawkins S, Keller AE, Koksal AC, Caceres CS, Berlin AA, Holoweckyj N *et al*: **PD-L1(+) neutrophils contribute to injury-induced infection susceptibility**. *Science advances* 2021, **7**(10).
15. Zhu CL, Xie J, Zhao ZZ, Li P, Liu Q, Guo Y, Meng Y, Wan XJ, Bian JJ, Deng XM *et al*: **PD-L1 maintains neutrophil extracellular traps release by inhibiting neutrophil autophagy in endotoxin-induced lung injury**. *Frontiers in immunology* 2022, **13**:949217.
16. Pan SW, Shu CC, Huang JR, Lee CC, Tseng YH, Hung JJ, Hsu PK, Chen NJ, Su WJ, Feng JY *et al*: **PD-L1 Expression in Monocytes Correlates with Bacterial Burden and Treatment Outcomes in Active Pulmonary Tuberculosis**. *International journal of molecular sciences* 2022, **23**(3).
17. Margaroli C, Horati H, Garratt LW, Giacalone VD, Schofield C, Dittrich AS, Rosenow T, Dobosh BS, Lim HS, Frey DL *et al*: **Macrophage PD-1 associates with neutrophilia and reduced bacterial killing in early cystic fibrosis airway disease**. *Journal of cystic fibrosis : official journal of the European Cystic Fibrosis Society* 2022, **21**(6):967-976.
18. Hartley GP, Chow L, Ammons DT, Wheat WH, Dow SW: **Programmed Cell Death Ligand 1 (PD-L1) Signaling Regulates Macrophage Proliferation and Activation**. *Cancer immunology research* 2018, **6**(10):1260-1273.
19. Ding Y, Yan Y, Dong Y, Xu J, Su W, Shi W, Zou Q, Yang X: **NLRP3 promotes immune escape by regulating immune checkpoints: A pan-cancer analysis**. *International immunopharmacology* 2022, **104**:108512.
20. Chen L, Huang CF, Li YC, Deng WW, Mao L, Wu L, Zhang WF, Zhang L, Sun ZJ: **Blockage of the NLRP3 inflammasome by MCC950 improves anti-tumor immune responses in head and neck squamous cell carcinoma**. *Cellular and molecular life sciences : CMLS* 2018, **75**(11):2045-2058.
21. Theivanthiran B, Evans KS, DeVito NC, Plebanek M, Sturdivant M, Wachsmuth LP, Salama AK, Kang Y, Hsu D, Balko JM *et al*: **A tumor-intrinsic PD-L1/NLRP3 inflammasome signaling pathway drives resistance to anti-PD-1 immunotherapy**. *The Journal of clinical investigation* 2020, **130**(5):2570-2586.
22. Ding X, Zhang J, Shi M, Liu D, Zhang L, Zhang R, Su B, Ai K: **High expression level of interleukin-1β is correlated with poor prognosis and PD-1 expression in patients with lung adenocarcinoma**. *Clinical & translational oncology : official publication of the Federation of Spanish Oncology Societies and of the National Cancer Institute of Mexico* 2021, **23**(1):35-42.
23. Takahashi R, Macchini M, Sunagawa M, Jiang Z, Tanaka T, Valenti G, Renz BW, White RA, Hayakawa Y, Westphalen CB *et al*: **Interleukin-1β-induced pancreatitis promotes pancreatic ductal**

adenocarcinoma via B lymphocyte-mediated immune suppression. *Gut* 2021, **70**(2):330-341.

24. He Q, Liu M, Huang W, Chen X, Zhang B, Zhang T, Wang Y, Liu D, Xie M, Ji X *et al*: **IL-1β-Induced Elevation of Solute Carrier Family 7 Member 11 Promotes Hepatocellular Carcinoma Metastasis Through Up-regulating Programmed Death Ligand 1 and Colony-Stimulating Factor 1**. *Hepatology (Baltimore, Md)* 2021, **74**(6):3174-3193.
25. Yuan B, Clowers MJ, Velasco WV, Peng S, Peng Q, Shi Y, Ramos-Castaneda M, Zarghooni M, Yang S, Babcock RL *et al*: **Targeting IL-1β as an immunopreventive and therapeutic modality for K-ras-mutant lung cancer**. *JCI insight* 2022, **7**(11).
26. Bartfai T, Behrens MM, Gaidarova S, Pemberton J, Shivanyuk A, Rebek J, Jr.: **A low molecular weight mimic of the Toll/IL-1 receptor/resistance domain inhibits IL-1 receptor-mediated responses**. *Proceedings of the National Academy of Sciences of the United States of America* 2003, **100**(13):7971-7976.
27. Matute-Bello G, Downey G, Moore BB, Groshong SD, Matthay MA, Slutsky AS, Kuebler WM: **An official American Thoracic Society workshop report: features and measurements of experimental acute lung injury in animals**. *American journal of respiratory cell and molecular biology* 2011, **44**(5):725-738.
28. Kulkarni HS, Lee JS, Bastarache JA, Kuebler WM, Downey GP, Albaiceta GM, Altemeier WA, Artigas A, Bates JHT, Calfee CS *et al*: **Update on the Features and Measurements of Experimental Acute Lung Injury in Animals: An Official American Thoracic Society Workshop Report**. *American journal of respiratory cell and molecular biology* 2022, **66**(2):e1-e14.
29. Wen Z, Ji X, Tang J, Lin G, Xiao L, Liang C, Wang M, Su F, Ferrandon D, Li Z: **Positive Feedback Regulation between Transglutaminase 2 and Toll-Like Receptor 4 Signaling in Hepatic Stellate Cells Correlates with Liver Fibrosis Post Schistosoma japonicum Infection**. *Frontiers in immunology* 2017, **8**:1808.
30. !!! INVALID CITATION !!! .
31. Arredouani MS, Palecanda A, Koziel H, Huang YC, Imrich A, Sulahian TH, Ning YY, Yang Z, Pikkarainen T, Sankala M *et al*: **MARCO is the major binding receptor for unopsonized particles and bacteria on human alveolar macrophages**. *Journal of immunology (Baltimore, Md : 1950)* 2005, **175**(9):6058-6064.
32. Kang MJ, Jang AR, Park JY, Ahn JH, Lee TS, Kim DY, Lee MS, Hwang S, Jeong YJ, Park JH: **IL-10 Protects Mice From the Lung Infection of Acinetobacter baumannii and Contributes to Bacterial Clearance by Regulating STAT3-Mediated MARCO Expression in Macrophages**. *Front Immunol* 2020, **11**:270.
33. Son K, Miyasaki K, Salter B, Loukov D, Chon J, Zhao N, Radford K, Huang C, LaVigne N, Dvorkin-Gheva A *et al*: **Autoantibody-mediated Macrophage Dysfunction in Patients with Severe Asthma with Airway Infections**. *American journal of respiratory and critical care medicine* 2023, **207**(4):427-437.
34. Gordon SR, Maute RL, Dulken BW, Hutter G, George BM, McCracken MN, Gupta R, Tsai JM, Sinha R, Corey D *et al*: **PD-1 expression by tumour-associated macrophages inhibits phagocytosis and tumour immunity**. *Nature* 2017, **545**(7655):495-499.
35. Wang Z, Hao C, Zhuang Q, Zhan B, Sun X, Huang J, Cheng Y, Zhu X: **Excretory/Secretory Products From Trichinella spiralis Adult Worms Attenuated DSS-Induced Colitis in Mice by Driving PD-1-**

Mediated M2 Macrophage Polarization. *Frontiers in immunology* 2020, **11**:563784.

36. Zong Z, Zou J, Mao R, Ma C, Li N, Wang J, Wang X, Zhou H, Zhang L, Shi Y: **M1 Macrophages Induce PD-L1 Expression in Hepatocellular Carcinoma Cells Through IL-1β Signaling**. *Frontiers in immunology* 2019, **10**:1643.
37. Antonangeli F, Natalini A, Garassino MC, Sica A, Santoni A, Di Rosa F: **Regulation of PD-L1 Expression by NF-κB in Cancer**. *Frontiers in immunology* 2020, **11**:584626.
38. Jin L, Batra S, Jeyaseelan S: **Deletion of Nlrp3 Augments Survival during Polymicrobial Sepsis by Decreasing Autophagy and Enhancing Phagocytosis**. *Journal of immunology (Baltimore, Md : 1950)* 2017, **198**(3):1253-1262.
39. Biswas R, Hamilton RF, Jr., Holian A: **Role of lysosomes in silica-induced inflammasome activation and inflammation in absence of MARCO**. *Journal of immunology research* 2014, **2014**:304180.
40. Ding L, Qian J, Yu X, Wu Q, Mao J, Liu X, Wang Y, Guo D, Su R, Xie H *et al*: **Blocking MARCO(+) tumor-associated macrophages improves anti-PD-L1 therapy of hepatocellular carcinoma by promoting the activation of STING-IFN type I pathway**. *Cancer letters* 2023, **582**:216568.
41. Freeman TL, Swartz TH: **Targeting the NLRP3 Inflammasome in Severe COVID-19**. *Frontiers in immunology* 2020, **11**:1518.
42. Hosseinian N, Cho Y, Lockey RF, Kolliputi N: **The role of the NLRP3 inflammasome in pulmonary diseases**. *Therapeutic advances in respiratory disease* 2015, **9**(4):188-197.
43. Pan P, Shen M, Yu Z, Ge W, Chen K, Tian M, Xiao F, Wang Z, Wang J, Jia Y *et al*: **SARS-CoV-2 N protein promotes NLRP3 inflammasome activation to induce hyperinflammation**. *Nature communications* 2021, **12**(1):4664.
44. Yang HH, Duan JX, Liu SK, Xiong JB, Guan XX, Zhong WJ, Sun CC, Zhang CY, Luo XQ, Zhang YF *et al*: **A COX-2/sEH dual inhibitor PTUPB alleviates lipopolysaccharide-induced acute lung injury in mice by inhibiting NLRP3 inflammasome activation**. *Theranostics* 2020, **10**(11):4749-4761.
45. Yuan R, Li Y, Han S, Chen X, Chen J, He J, Gao H, Yang Y, Yang S, Yang Y: **Fe-Curcumin Nanozyme-Mediated Reactive Oxygen Species Scavenging and Anti-Inflammation for Acute Lung Injury**. *ACS central science* 2022, **8**(1):10-21.
46. White A, Wang Z, Wang X, King M, Guo C, Mantsounga C, Ayala A, Morrison AR, Choudhary G, Sellke F *et al*: **NLRP3 inflammasome activation in cigarette smoke priming for Pseudomonas aeruginosa-induced acute lung injury**. *Redox biology* 2022, **57**:102467.

Highlights

- Acute *Sm* infection activated NLRP3 inflammasome and induced pyroptosis of macrophages, including alveolar macrophages.

- The expression of PD-1 and PD-L1, and the count of PD-1^+ or PD-$L1^+$, or $MARCO^+$

682 macrophages or PD-L1^{+}neutrophils in the lung with acute *Sm* infection were controlled
683 by NLRP3.

684

685 ● Bacterial load and acute lung injury in the mice with acute *Sm* pneumonia were
686 significantly correlated with the frequency of MARCO^{+} or PD-1^{+} macrophages and
687 IL-1β level, respectively.
688

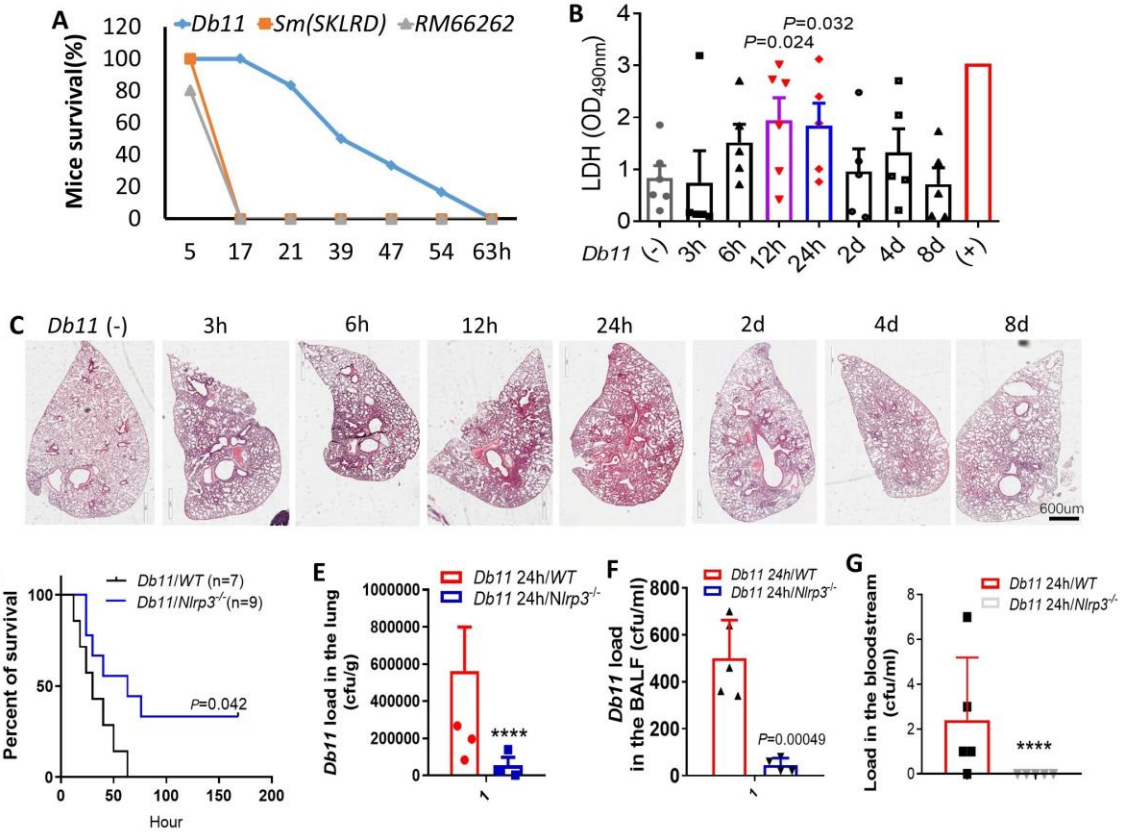

689

690 **Figure 1.** NLRP3 genetic deletion improved mice survival and lowered bacterial load. (A)
691 Survival rate of 5×10^7cfu of clinically isolated *Sm* strains, including *RM66262* (n=7) and
692 *SKLRD* (n=7) and the strain *Db11* (n=7) isolated from infecting *Drosophila*. (B) LDH level
693 in BALF of mice (n=5-6) with different time courses of *Db11* infection based on OD_{450}
694 was measured using a CytoTox96 non-radioactive cytotoxicity assay kit, and (+) meant
695 positive control. (C) Typical photograph of lung whole sections under H&E staining (n=5-
696 6). (D) Survival rate of *WT* (n=7), *Nlrp3*$^{-/-}$(n=8) mice with 5×10^7 cfu of *Db11* infection.
697 (E-G) Bacterial load in the lung (n=3), BALF (n=5) and bloodstream (n=5-6) of *WT* or

Nlrp3$^{-/-}$ mice with 5×10^6 cfu of *Db11* infection. Data were expressed as the mean ±SD of indicated numbers of mice from different groups (Kaplan–Meier curves and the log-rank test-Survival or Student's *t*-test, the statistic *P*-value was marked into the figures, * $P<0.05$, *** $P<0.001$ and **** $P<0.0001$).

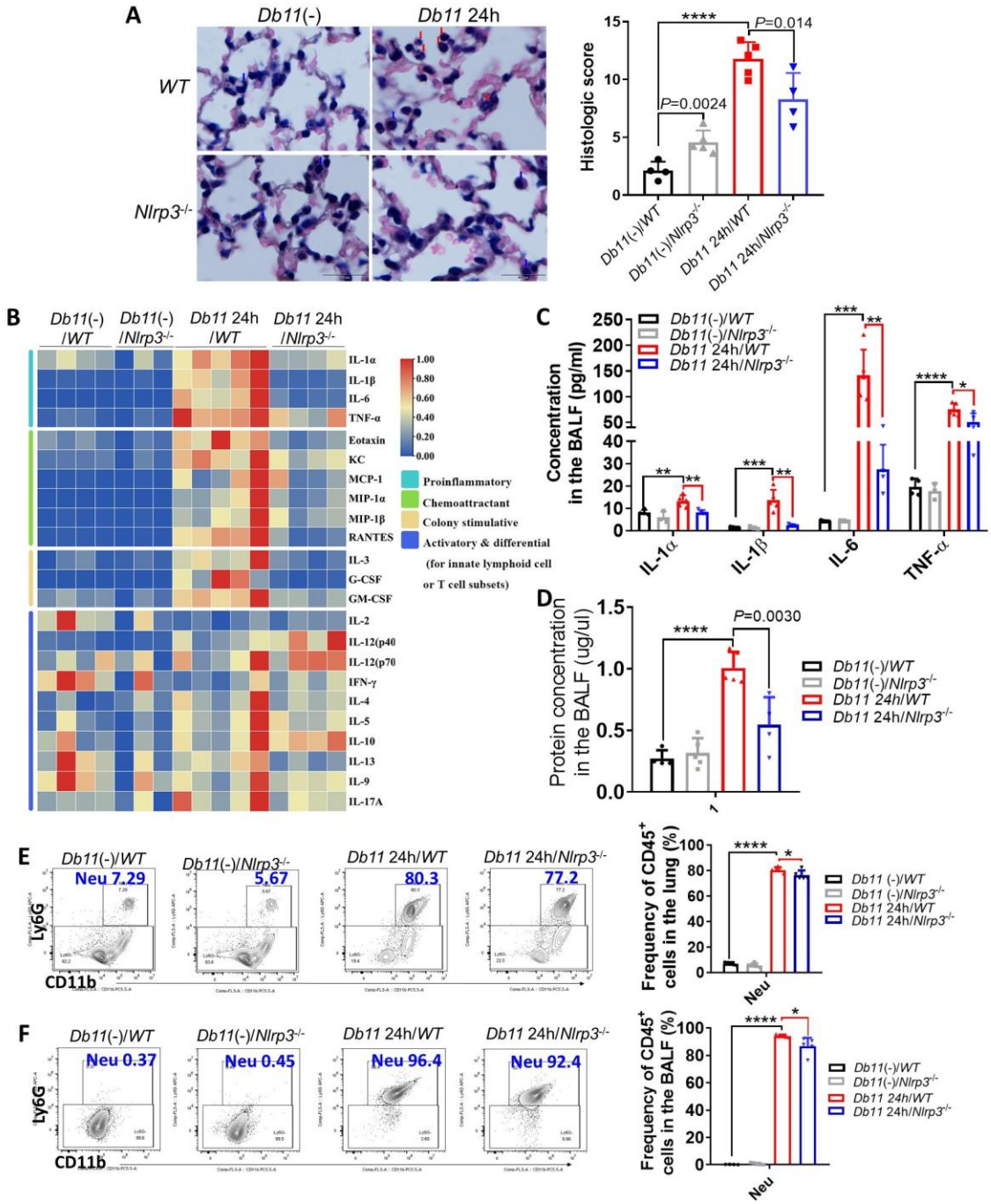

Figure 2. NLRP3 genetic deletion alleviated the severity of acute lung injury. (A) Typical

photograph of lung sections and the histologic score according to reported criteria from indicated mice (n=3-6) under H&E staining (macrophages or monocytes, blue arrows; neutrophils, red arrows). (B) Heatmap of 23 cytokines & chemokines level in BALF from indicated mice. (C) The concentration of IL-1α, IL-1β, IL-6, and TNF-α in BALF of indicated mice. (D) Concentration of total protein in BALF from indicated mice. Cells in the lung or BALF from non-infected and *Db11*-infected *WT* or *Nlrp3*$^{-/-}$ mice were harvested, and single cells were isolated and stained with dead-BV510, CD45, CD11b and Ly6G antibodies. Neu the lung (E) or in the BALF (F) were analyzed by flow cytometry and FlowJo software, representative gated cell populations, and their quantification was shown. Data were expressed as the mean ±SD of indicated numbers of mice from different groups (*WT* mice without *Db11* infection or *Db11*(-)/*WT*, n=4; *Nlrp3*$^{-/-}$ mice without *Db11* infection or *Db11*(-)/*Nlrp3*$^{-/-}$, n=3; *Db11* 24h/*WT*, n=5; *Db11* 24h/*Nlrp3*$^{-/-}$, n=4-5) (Student's *t*-test, Significant differences are indicated by * $P < 0.05$, ** $P< 0.01$, *** $P< 0.001$ and **** $P< 0.0001$).

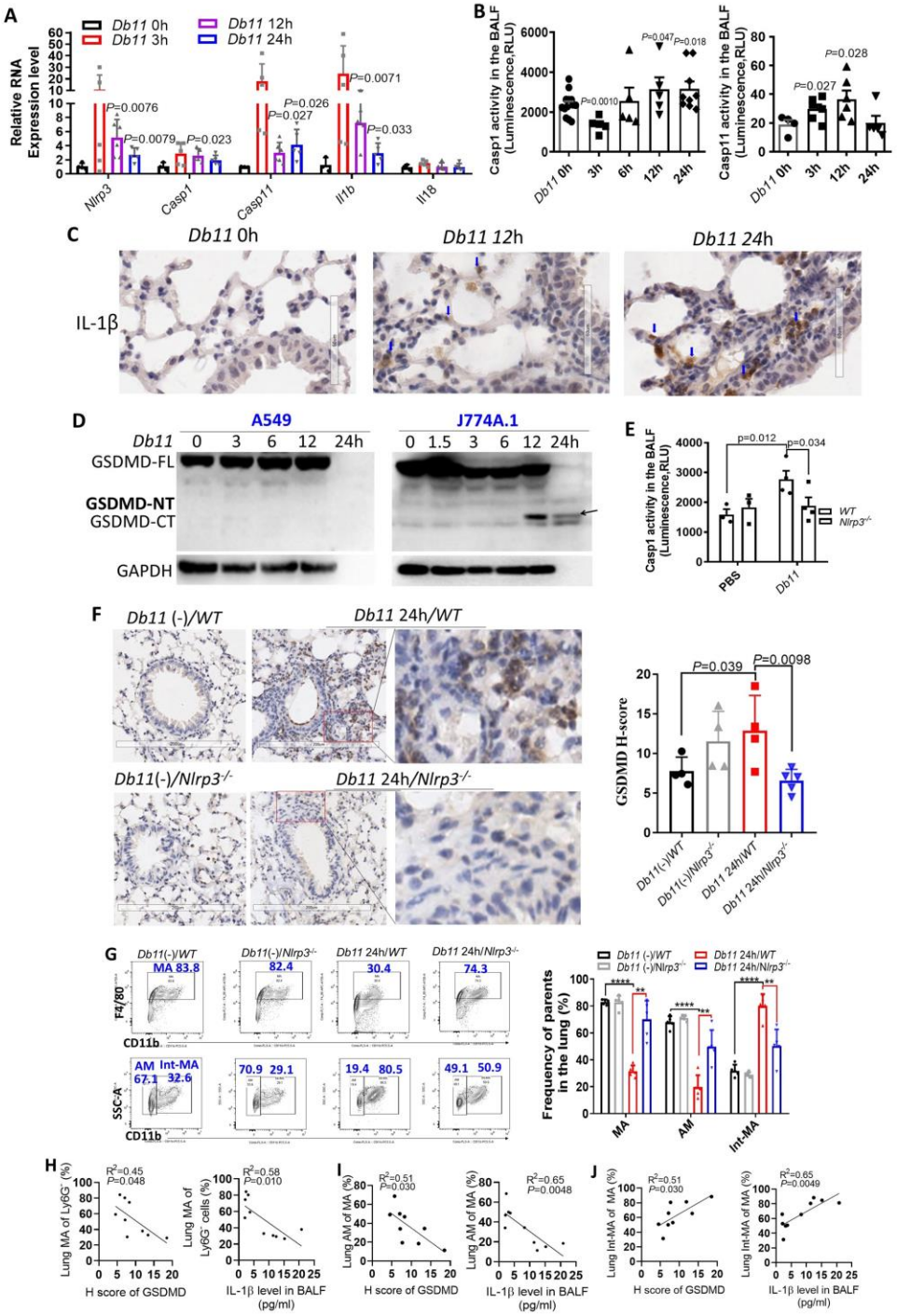

Figure 3. NLRP3 inflammasome in the macrophage was activated when acute *Db11* infection, and *Nlrp3* knockout recovered the count of alveolar macrophages but decreased the count of interstitial macrophages in the lung. (A) RT-qPCR was used to detect the transcription level of *Nlrp3*, *Casp1*, *Casp11* and *Il1b, Il18* in the *WT* mice lung with or without 5×10^6 cfu *Db11* infection (n=4-6). (B) Caspase-Glo 1/11 Inflammasome Assay

kit was used to detect the activity of Casp1 and Casp11 in BALF of *WT* mice with or without 5×10^6 cfu *Db11* infection (n=4-11). (C) IHC was used to detect the expression level and localization of IL-1β (blue arrow) in the lung of mice with or without 5×10^6 cfu *Db11* infection (n=4-6). (D) WB was used for GSDMD-FL and GSDMD-NT detection for A549 and murine MA J744A.1 with 5 multiplicity of infection (MOI) in indicated time courses. (E) Casp1 activity in BALF from indicated mice was detected by ELISA (n=3-4). (F) Expression level and localization of GSDMD in the lung of indicated mice (*Db11*(-)/*WT*, n=4; *Db11*(-)/*Nlrp3*$^{-/-}$, n=3; *Db11* 24h/*WT*, n=5; *Db11* 24h/*Nlrp3*$^{-/-}$, n=4-5) was determined by IHC. Representative photographs (left) and semi-quantitative H score (right) were shown. (G) Lungs from non-infected and 24h of *Db11*-infected *WT* or *Nlrp3*$^{-/-}$ mice (n=3-6) were harvested and single cells were prepared. These single cells were stained with dead-BV510, CD45, CD11b, Ly6G and F4/80 antibodies. CD45^{+}Ly6G^{-}F4/80^{+} cells (MA) and its subpopulation CD45^{+}Ly6G^{-}F4/80^{+} CD11b^{-} cells (alveolar macrophage, AM), CD45^{+}Ly6G^{-}F4/80^{+} CD11b^{+} cells (interstitial macrophage, Int-MA) were analyzed by flow cytometry and FlowJo software, representative gated cell populations (left) and their quantification (right) were shown. (H-J) Correlation of the frequency of lung MA of Ly6G^{-} cells, lung AM or Int-MA of MA with lung GSDMD expression level (H score of GSDMD) or with IL-1β level in the BALF was analyzed by Pearson's correlation test and presented as R^2 and *P*. Data were expressed as the mean ±SD of indicated numbers of mice from different groups (*Db11*(-)/*WT*, n=4; *Db11*(-)/*Nlrp3*$^{-/-}$, n=3; *Db11* 24h/*WT*, n=5; *Db11* 24h/*Nlrp3*$^{-/-}$, n=4-5) (Student's *t*-test). Statistic *P*-value was marked into the figures, * $P<0.05$; ** $P<0.01$ and **** $P< 0.0001$).

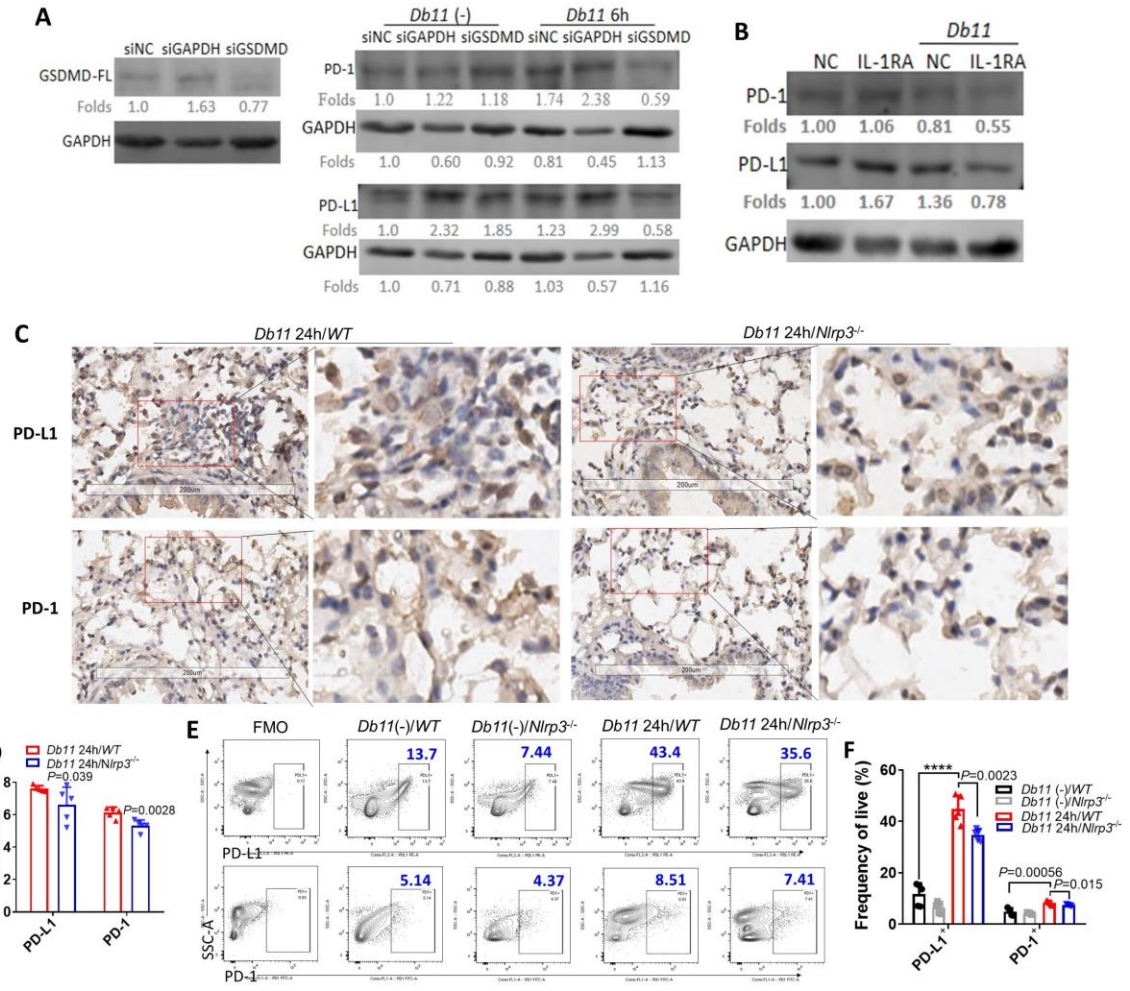

Figure 4. Inhibition of NLRP3 inflammasome decreased the expression of PD-1 and PD-L1 when acute *Db11* infection. (A) Effective siRNA of GSDMD was verified through WB, and siGAPDH was the quality control for the siRNA transfection kit (Left). WB was used to detect the expression level of PD-1 & PD-L1 in J744A.1 with or without siGSDMD transfection and then 5 MOI of *Db11* infection for 6 h, and non-infection as the control (right). (B) WB was used to detect the expression level of PD-1 & PD-L1 in J744A.1 with or without IL-1RA pretreatment for 30 min and then 5 MOI of *Db11* infection for 6h, and non-infection as the control. GAPDH worked as a loading control, and folds were calculated according to the Image J software analysis. (C-D) Expression level and localization of PD-L1 and PD-1 in the lung of indicated mice were determined by IHC. Representative photographs (C) and semi-quantitative H score (D) were shown. (E-F)

Single cells in the lung were stained with anti-PD-L1 and PD-1, and detected by flow cytometry. According to FlowJo software analysis, the frequency of PD-L1^{+} and PD-1^{+} cells of live cells in the lung were shown as representative populations (E) and quantitative frequency (F). Data were expressed as the mean ±SD of indicated numbers of mice from different groups (*Db11*(-)/*WT*, n=4; *Db11*(-)/*Nlrp3*$^{-/-}$, n=4; *Db11* 24h/*WT*, n=5; *Db11* 24h/*Nlrp3*$^{-/-}$, n=5) (Student's *t*-test, statistic *P*-value was marked into the figures, * $P<0.05$; ** $P<0.01$ and **** $P<0.0001$).

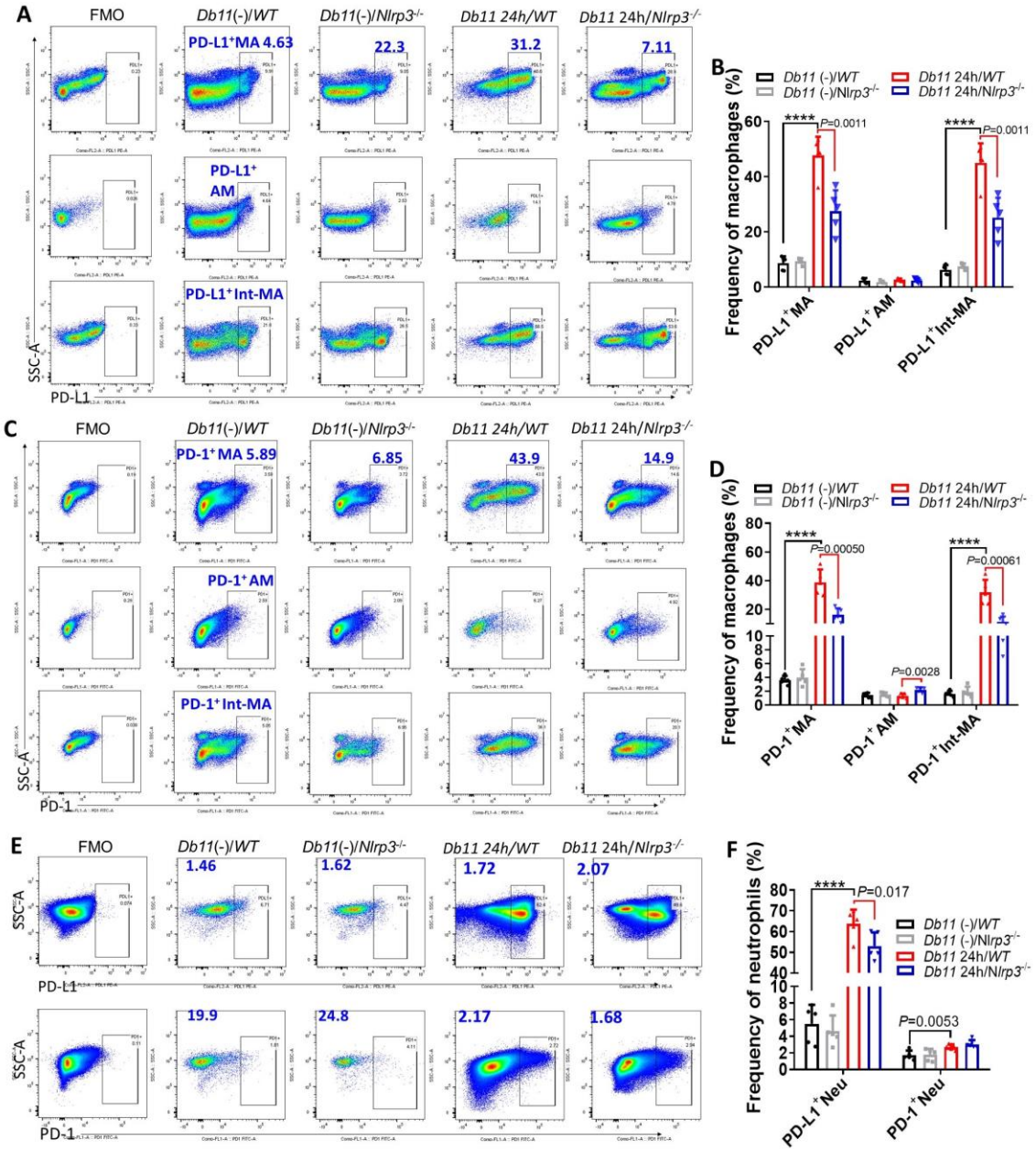

Figure 5. PD-L1$^+$, PD-1$^+$ macrophages and PD-L1$^+$ neutrophils were significantly decreased in the lung of *Sm*-infected *Nlrp3*$^{-/-}$ mice compared to *WT* mice.

(A-F) Single cells in the lung were stained with anti-PD-L1, PD-1, CD45, CD11b, Ly6G and anti-F4/80 and then were detected by flow cytometry. According to FlowJo software analysis, the frequency of PD-L1$^+$CD45$^+$Ly6G$^-$F4/80$^+$ (PD-L1$^+$MA) in CD45$^+$Ly6G$^-$F4/80$^+$ (MA) cells, PD-L1$^+$CD45$^+$Ly6G$^-$F4/80$^+$CD11b$^-$ (PD-L1$^+$ AM) in MA, or PD-L1$^+$CD45$^+$Ly6G$^-$F4/80$^+$ CD11b$^+$ (PD-L1$^+$ Int-MA) in MA were shown as representative

populations (A) and quantitative frequency (B). The frequency of PD-1$^+$MA in MA, PD-1$^+$ AM in PD-1$^+$MA, or PD-1$^+$ Int-MA in PD-1$^+$MA were shown as representative populations (C) and quantitative frequency (D). (E-F) Single cells in the lung were stained with anti-PD-L1, PD-1, CD45, CD11b and anti-Ly6G and then were detected by flow cytometry. According to FlowJo software analysis, the frequency of PD-L1$^+$CD45$^+$CD11b$^+$Ly6G$^+$(PD-L1$^+$Neu) in CD45$^+$CD11b$^+$Ly6G$^+$ (Neu), PD-1$^+$Neu in Neu were shown as representative populations (E) and quantitative frequency (F). Data were expressed as the mean ±SD of indicated numbers of mice from different groups (*Db11*(-)/*WT*, n=4; *Db11*(-)/*Nlrp3*$^{-/-}$, n=3; *Db11* 24h/*WT*, n=5; *Db11* 24h/*Nlrp3*$^{-/-}$, n=4-5) (Student's *t*-test, statistic *P*-value was marked into the figures, ** $P<0.01$; *** $P<0.001$ and **** $P<0.0001$).

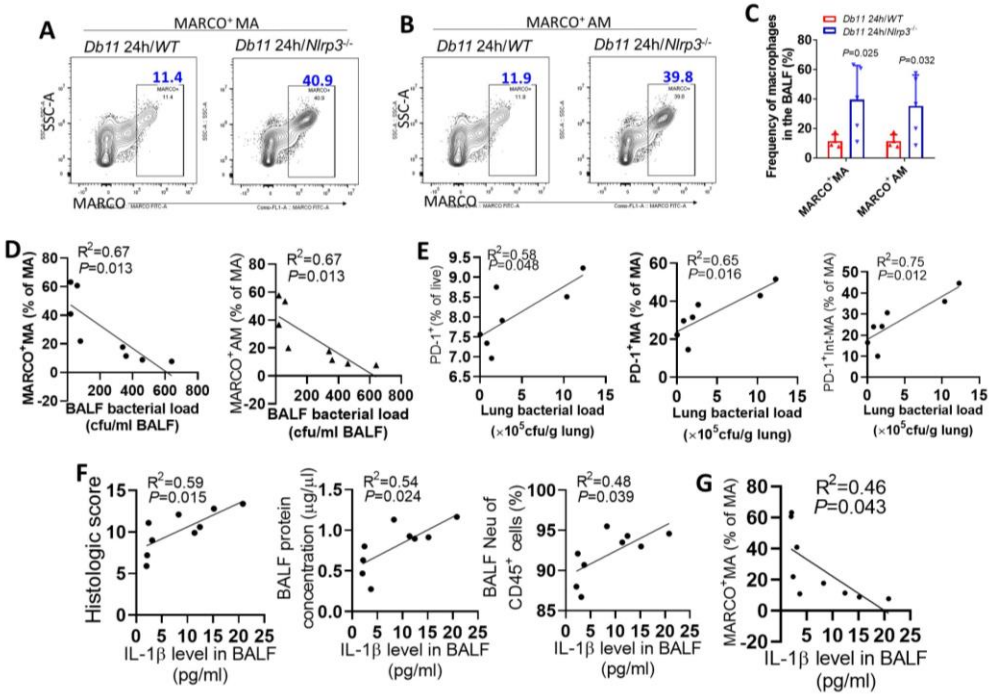

Figure 6. NLRP3-controlled acute *Sm* pneumonia was correlated with the frequency of MARCO$^+$ MA and PD-1 expression level especially the count of PD-1 expressing alveolar macrophages. (A-C) Single cells in the BALF were stained with anti-CD45, CD11b, Ly6G, F4/80 and anti-MARCO, and then were detected by flow cytometry. According to FlowJo

software analysis, the frequency of $CD45^+Ly6G^-F4/80^+MARCO^+$ ($MARCO^+MA$) in $CD45^+Ly6G^-F4/80^+$ cells (MA) (A), the frequency of $CD45^+Ly6G^-F4/80^+$ $CD11b^-$ $MARCO^+$ ($MARCO^+AM$) in MA (B) were shown as representative populations (A,B) and quantitative frequency (C). Correlation of the frequency of $MARCO^+MA$ and $MARCO^+AM$ of MA in BALF (D), $PD\text{-}1^+$ of live, $PD\text{-}1^+MA$, $PD\text{-}1^+$Int-MA of MA in the lung (E) with lung bacterial load were shown. Correlation of histologic score, BALF protein concentration or BALF Neu frequency of $CD45^+$ cells (G), or correlation of frequency of $MARCO^+MA$ of MA with IL-1β level in the BALF were shown. Pearson's correlation test was used and data were presented as R^2, and *P*. Data were expressed as the mean ±SD of indicated numbers of mice from different groups (*Db11*(-)/*WT*, n=4; *Db11*(-)/*Nlrp3*$^{-/-}$, n=3; *Db11* 24h/*WT*, n=5; *Db11* 24h/*Nlrp3*$^{-/-}$, n=4-5) (Student's *t*-test). Statistic *P*-value was marked into the figures, * $P<0.05$).

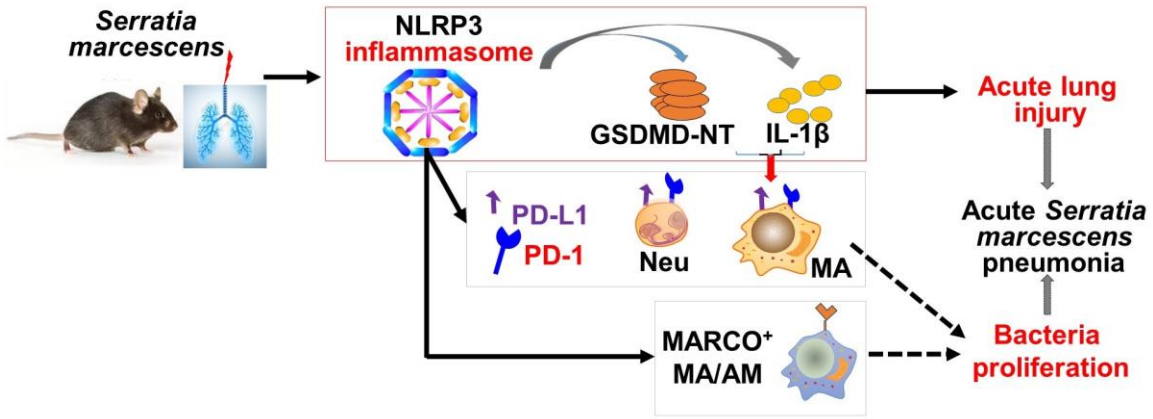

Graphical abstract

***Nlrp3* deletion protected against *Sm* infection-induced acute pneumonia.**

24 h of *Db11* infection in *WT* mice induced severe acute pneumonia, manifesting as acute lung injury and high bacterial proliferation through NLRP3 inflammasome activation and then GSDMD-NT-induced pyroptosis of alveolar macrophages and IL-1β secretion. Mechanistically, PD-L1 & PD-1 expression, the count of PD-L1 & PD-1 expressing macrophages, alveolar macrophages, interstitial macrophages, or PD-L1 expressing neutrophils, and the count of $MARCO^+$ macrophages especially $MARCO^+$ alveolar

816 macrophages were controlled by NLRP3 or NLRP3 inflammasome. Note: Arrows with
817 solid lines made sure in this project; arrows with dash lines reported by references or
818 correlation analysis.
819